

Exploring the Galactic Anticenter Substructure with LAMOST and Gaia DR2

Jing Li^{1,2,12}, Xiang-Xiang Xue^{3,5,11}, Chao Liu^{4,5}, Bo Zhang⁶, Hans-Walter Rix⁷, Jeffrey L. Carlin⁸, Chengqun Yang⁹, Rene A. Mendez¹⁰, Jing Zhong⁹, Hao Tian⁴, Lan Zhang³, Yan Xu³, Yaqian Wu³, Gang Zhao^{3,5}, and Ruixiang Chang⁹

Max-Planck-Institut für Astronomie, Königstuhl 17, D-69117 Heidelberg, Germany AURA/Rubin Observatory, 950 North Cherry Avenue, Tucson, AZ 85719, USA

Abstract

We characterize the kinematic and chemical properties of 589 Galactic anticenter substructure stars (GASS) with K/M giants in integrals-of-motion space. These stars likely include members of previously identified substructures such as Monoceros, A13, and the Triangulum-Andromeda cloud. We show that these stars are in nearly circular orbits on both sides of the Galactic plane. We can see a velocity (V_Z) gradient along Y-axis especially for the south GASS members. Our GASS members have similar energy and angular momentum distributions to thin-disk stars. Their location in $\lceil \alpha/M \rceil$ versus $\lceil M/H \rceil$ space is more metal-poor than typical thin-disk stars, with $\lceil \alpha/M \rceil$ lower than that of the thick disk. We infer that our GASS members are part of the outer metal-poor disk stars and that the outer disk extends to 30 kpc. Considering the distance range and α -abundance features, GASS could be formed after the thick disk was formed due to the molecular cloud density decreasing in the outer disk where the star-formation rate might be less efficient compared to the inner disk.

Unified Astronomy Thesaurus concepts: Milky Way stellar halo (1060); Milky Way disk (1050); Stellar kinematics (1608); Chemical abundances (224)

Supporting material: machine-readable tables

1. Introduction

1.1. Historical Overview of Galactic Anticenter Substructure Stars

The low Galactic latitude substructures collectively known as "The Monoceros Ring" (hereafter referred to as Mon) were first discovered by Newberg et al. (2002). Four stellar overdensities were identified at low latitude—those labeled S223+20-19.4, S218+22-19.5, and S183+22-19.4 located in the north Galactic cap, and S200-24-19.8 found below the plane. All of these detections are within 40° of the Galactic anticenter at (l, b) =(180°, 0°). The turnoffs of the faint main sequence of these overdensities are significantly bluer than the turnoff of typical thick-disk stars. Newberg et al. (2002) interpreted the bluer turnoff as evidence of a more metal-poor population, as had been identified in the Sagittarius dwarf tidal stream, though the effect could also be due to a population with a younger stellar age.

Within a year, Yanny et al. (2003) and Ibata et al. (2003) suggested that the low-latitude structure was ring-like and could potentially encircle the entire galaxy (this same structure has been referred to as the Galactic anticenter stellar structure, or GASS, by Rocha-Pinto et al. 2003 and subsequent work). Yanny et al. (2003) traced the structure from $180^{\circ} < l < 227^{\circ}$ and noted that it extended 5 kpc above and below the Galactic plane, though the southern portion was 2 kpc farther away. They found a velocity dispersion of $\sim 25 \,\mathrm{km \, s^{-1}}$, which is lower than that of the thick disk (typically 40–50 km s⁻¹), and a scale height that is larger than the thick disk. Based on these observations, Yanny et al. (2003) argued that "the Monoceros ring" is a tidal stream. Simultaneously, Ibata et al. (2003) pointed out that the ring was not actually traced around the entire Galaxy, but was detected in the range $120^{\circ} < l < 200^{\circ}$, on both sides of the Galactic plane. This suggests that the ring could be an artifact in the disk caused by repeated warping, a tidal stream from an accreted satellite, or part of an outer spiral arm. In the same year, Rocha-Pinto et al. (2003) showed that the ring was visible in 2MASS M-giant stars, establishing that there is a range of metallicities present in this structure, and believed it was the result of a tidally disrupting dwarf galaxy (for more details about Monoceros/GASS, see Yanny & Newberg 2016 and other chapters in Newberg & Carlin 2016).

Several authors have raised the hypothesis of a flare and warp of the outer disk to explain the Monoceros Ring (López-Corredoira et al. 2002; Moitinho et al. 2006; Momany et al. 2006; Carraro & Costa 2009; Hammersley & López-Corredoira 2011;

¹ Physics and Space Science College, China West Normal University, 1 ShiDa Road, Nanchong 637002, People's Republic of China; lijing@bao.ac.cn ² Chinese Academy of Sciences South America Center for Astronomy, National Astronomical Observatories, Chinese Academy of Sciences, Beijing 100101, People's Republic of China

³ CAS Key Laboratory of Optical Astronomy, National Astronomical Observatories, Chinese Academy of Sciences, Beijing 100101, People's Republic of China; xuexx@nao.cas.cn

⁴ Key Laboratory of Space Astronomy and Technology, National Astronomical Observatories, Chinese Academy of Sciences, Beijing 100101, People's Republic of China

⁵ School of Astronomy and Space Science, University of Chinese Academy of Sciences, 19A Yuquan Road, Shijingshan District, Beijing 100049, People's Republic of China

⁶ Department of Astronomy, Beijing Normal University, Beijing 100875, People's Republic of China

⁹ Key Laboratory for Research in Galaxies and Cosmology, Shanghai Astronomical Observatory, Chinese Academy of Sciences, 80 Nandan Road, Shanghai 200030, People's Republic of China

¹⁰ Departamento de Astronomia, Universidad de Chile, Casilla 36-D, Correo Central, Santiago, Chile Received 2019 October 24; revised 2021 January 4; accepted 2021 January 5; published 2021 March 25

¹¹ First corresponding author.

¹² Second corresponding author.

Feast et al. 2014). However, this idea has difficulties explaining the narrow radial velocity dispersion of Mon (Meisner et al. 2012).

An extensive photometric and spectroscopic study using SDSS, including SEGUE and SEGUE-2 spectroscopy in the anticenter region, was carried out by Li et al. (2012). They conclude that the Monoceros structure has a metallicity of [Fe/H] $\sim -0.80 \pm 0.1$, and the ring has a higher metallicity than the halo, but slightly lower metallicity and a narrower velocity dispersion than the thick disk. All kinematics of Monoceros stars, however, show prograde motion, rotating with the disk, and not far in velocity from the circular motion of stars in a flat rotation curve.

Subsequently, the Pan-STARRS1 survey presented a panoramic picture of the anticenter in stellar density above and below the Milky Way plane. Figure 2 of Slater et al. (2014) clearly shows the "band-like" structure stretching from $l=100^\circ$ to 230° , and covering a large Galactic latitude range of $-35^\circ < b < 35^\circ$ in some regions.

Detailed studies of chemical abundances in Mon/GASS have been carried out by Chou et al. (2010) and Meisner et al. (2012). Chou et al. (2010) derived chemical abundance patterns from high-resolution spectra of 21 M giants. The abundances of the α -element titanium, and the *s*-process elements yttrium and lanthanum, for these GASS stars are found to be lower at the same [Fe/H] than those for Milky Way stars, but similar to those of stars in the Sagittarius stream, other dwarf spheroidal galaxies, and the Large Magellanic Cloud. From low-resolution ($R \sim 1000$) data for hundreds of F/G stars in the anticenter at distances dominated (65%) by objects in Mon/GASS, Meisner et al. (2012) found [Fe/H] ~ -1 , which is intermediate between the halo and the local thick disk. They also found significantly different metallicities for stars at the same Galactocentric radii above and below the plane ([Fe/H] = -0.65 versus -0.87 dex, respectively).

Xu et al. (2015) showed that there is a vertical asymmetry in the disk that is a function of distance from the Galactic center, as measured in the direction of the anticenter. They think the oscillation lines up with the position and density of the Mon and Triangulum-Andromeda cloud (TriAnd) structures, but it is only apparent in the north. There are excess star counts in both the north and the south, but they are at different Galactocentric distances.

Li et al. (2017) presented an analysis of spectroscopic observations of individual stars from "A13," which they concluded based on positions, distances, and kinematical properties to be an extension of Mon. Sheffield et al. (2018) studied the stellar population of Mon, A13, and TriAnd to assess the relative numbers of RR Lyrae and M-giant stars, and found that both structures have very low $f_{RR:MG}$, supporting the scenario in which stars in Mon, A13, and TriAnd formed in the Milky Way disk.

1.2. Historical Overview of MWTD in the Context of the Milky Way

The existence of a metal-weak thick-disk (MWTD) population has been confirmed in the past two decades. The first paper about MWTD was from Norris et al. (1985), which presented a sample of 309 non-kinematically weak-metal candidates in the solar neighborhood. Follow-up research suggested that the low-metallicity and low-eccentricity stars belong to a population that is intermediate in its motion perpendicular to the Galactic plane between that of the thin disk and that of metal-deficient

objects of extreme eccentricity, and the velocity dispersion of this group of stars is consistent with the thick disk (Morrison et al. 1990; Beers et al. 1995).

Other observational efforts, including high-/medium-resolution spectroscopic abundance determinations, have addressed the problem (the fractions of stars at low metallicity were substantially smaller) of the existence of an MWTD component in the solar neighborhood of the Galaxy (Beers & Sommer-Larsen 1995; Chiba & Yoshii 1998; Martin & Morrison 1998; Beers et al. 2000; Arifyanto et al. 2005). Some authors interpreted the origin of the MWTD in terms of the debris of a "shredded satellite" (Gilmore et al. 2002; Arifyanto et al. 2005). The preponderance of evidence acquired prior to 2009 suggested that an MWTD component exists in the solar neighborhood, although these analyses generally did not consider stars with such a large lag as likely candidate disk-like stars, as argued by Villalobos & Helmi (2009).

In the period since 2009, a substantial volume of work has been carried out, making use of large samples of stars with medium-resolution ($R \sim 2000$) spectroscopy obtained from a variety of surveys, in particular the Sloan Digital Sky Survey (SDSS; York et al. 2000), as well as the higher-resolution $(R \sim 7500)$ data from the Radial Velocity Experiment (Steinmetz et al. 2006) and other sources. During this period, our appreciation of the complexity of the halo has also increased. Carollo et al. (2007, 2010), and Beers et al. (2012) have presented the case that this system is well-described in terms of an inner-halo and outer-halo population. Additional evidence supports the existence of (at least) a dual halo around the frequency of carbon-enhanced metal-poor stars, metallicity distribution function, and so on (Carollo et al. 2012, 2014; An et al. 2013). Furthermore, Morrison et al. (2009) studied 250 stars in the presence of a new component of the local halo, with the axial ratio similar in flattening to the thick disk and populated by stars -1.5 < [Fe/H] < -1.0, although not rotationally supported. Beers et al. (2014), using a new set of very high signal-to-noise ratio (S/N > 100/1), medium-resolution $(R \sim 3000)$ optical spectra obtained for 302 of the candidate "weak-metal" stars selected by Bidelman & MacConnell (1973), this work proved the presence of MWTD population, and found 25% of the stars with metallicities -1.8 < [Fe/H] < -0.8 exhibit orbital eccentricities e < 0.4, yet are clearly separated from members of the inner-halo population with similar metallicities. These works have raised new and interesting questions concerning the nature of the formation and evolution of both the disk and halo systems which need a large spectroscopic data to arrive at a widely accepted view.

The second data release of the Gaia mission (Gaia Collaboration et al. 2018), in combination with a large sample of spectroscopic surveys, provides the opportunity to search the Galactic halo substructures in a wide view in 7D phase space (i.e., 6D positions+velocities, plus metallicities). X.-X. Xue et al. (2021, in preparation) identified substructures with high reliability in energy versus angular momentum space with K/M giants selected from the LAMOST spectroscopic survey and Gaia DR2. From these large groups of substructures, we found four ring-like groups around the Galactic anticenter, with kinematic features similar to the GASS. In this paper, we present the kinematic and chemical features of these groups. The paper is organized as follows. In Section 2, we describe LAMOST K-/M-giant stars and the integrals-of-motion (I.o.M) and friends-of-friends (FoF) algorithm. The kinematic features

of GASS stars are described in Section 3. We present the chemical abundance features in Section 4. The discussion and conclusion are presented in Section 5.

2. Data and Method

2.1. Data

The data used in this work consist of spectroscopically identified K and M giants from LAMOST Data Release 5 (DR5). The LAMOST Telescope is a 4 m Schmidt telescope at Xinglong Observing Station. This National Key Scientific facility built by the Chinese Academy of Sciences (Cui et al. 2012; Deng et al. 2012; Luo et al. 2012; Zhao et al. 2012) has finished the first stage of its regular survey (LAMOST-I, from 2011–2017; including the pilot survey), and provided 9,027,634 low-resolution ($R \sim 1800$) optical spectra in its fifth data release, of which 8,183,667 are stellar spectra.

K-giant stars are selected from LAMOST DR5 according to the criteria presented in Liu et al. (2014; (4000 K < $T_{\rm eff}$ < 4600 K and log g < 3.5)||(4600 K < $T_{\rm eff}$ < 5600 K and log g < 4)). The distances of K giants are estimated following the Bayesian method described in Xue et al. (2014), which is suitable for the distance estimation of halo K giants due to the adopted fiducials of globular clusters. The typical distance precision of LAMOST halo K giants is 13% (Bird et al. 2019; Yang et al. 2019a).

M-giant stars are from Zhong et al. (2019), which used a spectroscopic template-matching method plus 2MASS+WISE photometric selection to identify 40,000 M giants from LAMOST DR5. The contamination of the M-giant sample by 894 carbon stars has also been excluded by cross-matching with the latest LAMOST carbon star catalog (Ji et al. 2016; Li et al. 2018). The distances of M giants were calculated through the $(J - K)_0$ color distance relation derived by Li et al. (2016).

Because the distances of K and M giants are derived using different calculation methods and calibration with distant stars, we recalibrated the distances of K and M giants by the Gaia DR2 parallax rather than Gaia distances estimated by Bailer-Jones et al. (2018). Bailer-Jones et al. (2018) claimed that their mean distances to distant giants are underestimated, due to the stars having very large fractional parallax uncertainties because their distances are prior-dominated, and the prior was dominated by the nearer dwarfs in the model. Only stars with good parallaxes $(\delta \varpi / \varpi < 20\%)$ and good distances $(\delta d / d < 20\%)$ are used to do the calibration, which allows us to compare the parallax with 1/dand minimize the possible bias from inverting. Finally, we used halo stars (the sample for which all the identified group members have been deleted) selected out from X.-X. Xue (2021, in preparation) as the calibration sample. For K and M giants, there is a 15% and 30% bias, respectively (for details, see Figure 1 of Yang et al. 2019b). Therefore, we increase the distances of K giants by $(1/0.85-1) \sim 18\%$ and decreased the distance of M giants by 30%.

The proper motions of the K and M giants are obtained by cross-matching with Gaia DR2 within less than 1". LAMOST pipeline provides the heliocentric radial velocities hrv with the typical error of $7 \, \mathrm{km}^{-1}$. The chemical abundances (metallicity [M/H] and abundance of α elements [α /M]) of LAMOST K and M giants are from Zhang et al. (2019), who used a machine-learning program called Stellar LAbel Machine (SLAM) to transfer APOGEE (Majewski et al. 2017) stellar labels to LAMOST DR5 spectra. The corresponding cross-validated

scatters of [M/H] and [α /M] at high signal-to-noise ratio (S/N_g ~100) are 0.037 dex and 0.026 dex. All stars for K and M giants underwent the initial cut; only stars at |Z| > 5 kpc and those with 2 kpc < |Z| < 5 kpc and [M/H] < -1 are classified as halo stars, which we will use to identify substructures in the following section. The disk stars we used in this work as a comparison with our GASS members are selected from LAMOST K giants for which |Z| < 3 kpc (details in Section 3.3).

2.2. Identification of Galactic Anticenter Substructure

Substructure in the Galaxy can be taken as stars moving in similar orbits, but possibly in quite different orbital phases. The orbit can be characterized by its I.o.M. Under the assumption that the potential of the Galactic halo, in the simplest approximation, is relatively spherical, there are four I.o.M.: the energy E and the angular momentum vector $L(L_x, L_y)$, and L_z). As described in Yang et al. (2019b), X.-X. Xue et al. (2021, in preparation) identified Galactic substructure by grouping stars with similar E and L from LAMOST K/M giants, SEGUE K giants, and SDSS Blue Horizontal Branch (BHB) stars. Specifically, the E and L can be translated to eccentricity e, semimajor axis a, the direction of the orbital pole $(l, b)_{\text{orbit}}$, and the direction of apocenter l_{apo} (i.e., the angle between the apocenter and the projection of x-axis on the orbital plane). Please note that $l_{\rm apo}$ changes with the period but remains constant within one period, which can be used to distinguish stars in the same stream but involving in our Galaxy in different epochs (e.g., Sgr leading and trailing arms).

By defining the orbit-likelihood distance to measure how closely two stars are distributed in I.o.M. space, X.-X. Xue et al. (2021, in preparation) applied the FOF algorithm to link stars moving in similar orbits together, where the choice of "linking length" is to make sure Sgr streams can be identified as completely as possible.

There are four data set used in the Xue et al. work to identify halo substructures, including LAMOST K giants and M giants, SEGUE K giants, and SDSS BHBs. Finally, X.-X. Xue et al. (2021, in preparation) identified 27 groups from LAMOST K/M giants and SDSS K giants and BHB stars with group members larger than 50. By comparing the sky coverage of these groups, we find four groups from LAMOST K/M giants located in the Galactic anticenter that share the same kinematic and chemical properties. Two of these four groups are from the K-giant sample, and the others from the M-giant sample. Their location in Galactic coordinates can be seen in Figure 1. These four groups share similar kinematic and chemical features on the two sides of the Galactic disk (in the following section, we will discuss the kinematic and chemical features in detail). If we relax the restriction of link length from the FoF method in X.-X. Xue et al. (2021, in preparation), the two groups of K giants will merge into one group because they are located on two sides of the Galactic disk; this condition is the same for two groups of M giants. Considering that these four groups also share the same kinematic and chemical properties, we infer that they belong to the same structure. By comparing these candidates with results from various works (Newberg et al. 2002; Ibata et al. 2003; Yanny et al. 2003; Li et al. 2012; Slater et al. 2014), we find that our candidates actually include at least the three components: Mon, A13, and Triand. Mon is the ring-like substructure detected in the lower latitudes near the Galactic anticenter, with a line-of-sight velocity similar to the thick disk but with a much smaller velocity dispersion (Newberg et al. 2002; Yanny et al. 2003; Li et al. 2012).

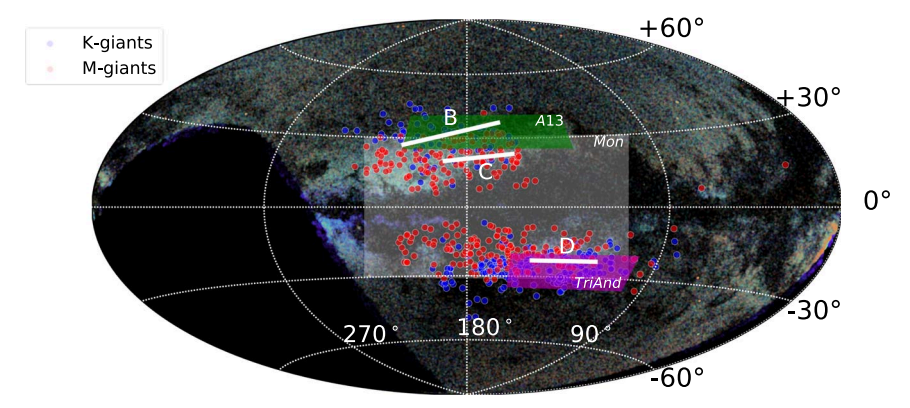


Figure 1. Sky coverage of our GASS members in Galactic coordinates. The blue and red filled circles show our GASS members with K/M giants. The background shows the sky coverage map of main-sequence turnoff stars from the Pan-STARRS catalog with $0.2 < (g - r)_0 < 0.3$. Nearby stars with $17.8 < g_0 < 18.4$ (4.8–6.3 kpc) are shown in blue, stars with $18.8 < g_0 < 19.6$ (7.6–11.0 kpc) are shown in green, and more distant stars with $20.2 < g_0 < 20.6$ (14.4–17.4 kpc) are shown in red. The green/white/purple square regions show previously detected A13, Mon, and TriAnd regions.

A13 is a substructure found to the north of the Galactic plane in the anticenter direction, with heliocentric distance $\sim\!10\text{--}20\,\mathrm{kpc}$, line-of-sight velocity distribution similar to the disk, and [Fe/H] $\sim\!-0.4$ to 0.8 dex (Sharma et al. 2010; Li et al. 2017). The TriAnd overdensity is found below the Galactic plane near the anticenter direction, with heliocentric distance $\sim\!10\text{--}25\,\mathrm{kpc}$, line-of-sight velocity distribution similar to a disk model with rotation velocity 150 km s $^{-1}$, and distance $\sim\!20\,\mathrm{kpc}$ (Deason et al. 2014). The truth is that there are many substructures in the Galactic anticenter region, and many of them overlap in their properties (e.g., spatial distribution, kinematics, and chemical abundances). Our work collects them all as one group with K/M giants.

Throughout this work, we refer to the collection of these structures as GASS, with the caveat that the features may not all be part of the same structure. In the next section, we will examine the features of these candidates in detail, including spatial, kinematic, and chemical abundance features. The observational parameters and calculated orbital parameters of the 589 GASS members are listed in Tables 1 and 2 separately. In what follows, we will further explore the nature of GASS using this sample.

3. The Kinematic Features of GASS

3.1. Spatial Distribution

Figure 1 summarizes the Galactic distribution of the selected GASS members. The members cover a large area on two sides of the disk near the Galactic anticenter, spanning the range $90^{\circ} < l < 230^{\circ}$ and $-40^{\circ} < b < 40^{\circ}$. We further compare the positions of these stars with the density map of the main-sequence turnoff stars from the work of Slater et al. (2014) based on the Pan-STARRS catalog. Figure 1 is similar to Figure 3 from Slater et al. (2014), but using colored dots that label stars at different distances. Our GASS members have good positional alignment with the "band-like" structures in the Pan-STARRS map. It is worth noting that our sample is in good agreement with the GASS features highlighted in their paper (see, e.g., features B, C, and D in Figure 3 of Slater et al. 2014). We also labeled the previously detected Mon, A13 and TriAnd regions with white, green, and purple squares separately as a comparison.

3.2. The Phase-space Distribution

For the measurement errors of our sample, LAMOST K giants have a median distance precision of 13% (Xue et al. 2014), a median radial velocity error of $7\,\mathrm{km\,s}^{-1}$, a median

error of 0.14 dex in metallicity, and a median $[\alpha/Fe]$ error of 0.05 dex (Liu et al. 2014; Zhang et al. 2019). LAMOST M giants have a typical distance precision of 20%, but do not have estimates of the distance error for each star (Li et al. 2016). LAMOST M giants have typical radial velocity errors of about 5 km s⁻¹ (Zhong et al. 2019), a median error of 0.17 dex in metallicity, and a median $[\alpha/\text{Fe}]$ error of 0.06 dex (Zhang et al. 2019). The proper motions of K giants and M giants are derived from Gaia DR2, which is good to 0.2 mas yr⁻¹ at $G = 17^{m}$. In this work, we calculate the errors of each calculated parameter for all K/M giants, based on the observational parameters (such as radial velocity, pmra, pmdec, and heliocentric distance) using a Markov Chain Monte Carlo method. This involves running our algorithm 1000 times for every single star, sampling from the parameter error distributions (assumed to be Gaussian) to get per-star errors for the different parameters. With these parameters and corresponding errors, we are able to analyze the phase-space distribution of the 589 GASS members; the parameters and corresponding errors can be found in Tables 1 and 2. Xu et al. (2015) proposed that Mon (close to the Sun) and TriAnd (farther from the Sun) could be associated with the same locally apparent disturbance, as the northern and southern parts of a vertically oscillating ring propagating outward from the Galactic center. Gómez et al. (2016) and Laporte et al. (2018) using N-body and/or hydrodynamical simulations have shown that Milky Way satellites could produce strong disturbances and might lead to the formation of vertical structure in the Galactic disk. Some observational work has also shown that there exists a ripple pattern and perturbed velocities in the disk within $r_{\rm gc}$ < 12 kpc (Liu et al. 2017; Antoja et al. 2018; Binney & Schönrich 2018; Tian et al. 2018; Bland-Hawthorn et al. 2019; Cheng et al. 2019; Laporte et al. 2019; Xu et al. 2020). Figure 8 from Li et al. (2017) schematically illustrates a possible scenario where Mon, A13, and TriAnd are the signatures of disk oscillations at different Galactocentric distances.

Figure 2 shows projections of the 3D distribution of our GASS samples onto the Galactic X-Y and r-Z planes. ¹³ In the left panel, the arrows indicate the direction and amplitude of the

 $[\]overline{^{13}}$ The Cartesian reference frame used in this work is centered at the Galactic center, the *X*-axis is positive toward the Galactic center, the *Y*-axis is along the rotation of the disk, and the *Z*-axis points toward the north Galactic pole. The Sun's position is at (-8.3, 0, 0) kpc (de Grijs & Bono 2016), the local standard of rest (LSR) velocity is 225 km s⁻¹ (de Grijs & Bono 2017), and the solar motion is (+11.1, +12.24, +7.25) km s⁻¹ (Schönrich et al. 2010).

| LAMOST ^a | Gaia ^b | Туре | R.A. (deg) | Decl. (deg) | d (kpc) | Δd (kpc) | hrv (km s ⁻¹) | Δhrv (km s ⁻¹) | pmra (mas yr ⁻¹) | Δ pmra (mas yr ⁻¹) | pmdec (mas yr ⁻¹) | Δ pmdec (mas yr ⁻¹) | [M/H] (dex) | Δ [M/H] (dex) | [\alpha/M] (dex) | $\Delta[\alpha/M]$ (dex) |
|---------------------|---------------------|-----------|---------------|----------------|------------|------------------|------------------------------|------------------------------------|---------------------------------|---------------------------------------|----------------------------------|--|----------------|----------------------|------------------|--------------------------|
| 216068 | 352530915661312 | LAMOST KG | 44.017706 | 0.962512 | 15.6 | 1.6 | 1.7 | 5.1 | 0.142 | 0.082 | -0.967 | 0.076 | -0.21 | 0.11 | 0.04 | 0.05 |
| 715099 | 2872282645040005120 | LAMOST KG | 352.857183 | 32.318859 | 19.2 | 2.8 | -171.9 | 5.5 | -0.72 | 0.082 | -0.929 | 0.059 | -0.79 | 0.23 | 0.07 | 0.07 |
| 716170 | 2872538315852901632 | LAMOST KG | 352.093575 | 32.856964 | 15.3 | 2.5 | -145.5 | 6.7 | -1.055 | 0.074 | -0.926 | 0.056 | -0.40 | 0.23 | -0.07 | 0.07 |
| 1107119 | 115451783231530112 | LAMOST KG | 47.05329 | 26.617279 | 14.6 | 2.1 | -44.4 | 6.8 | 0.205 | 0.204 | -0.571 | 0.141 | -0.77 | 0.22 | 0.11 | 0.07 |
| 1202158 | 1888486850788253056 | LAMOST KG | 337.893154 | 29.742142 | 20.6 | 1.3 | -199.0 | 4.7 | -1.203 | 0.077 | -1.081 | 0.084 | -1.0 | 0.19 | 0.04 | 0.07 |
| 1216219 | 1901404634945395456 | LAMOST KG | 338.411149 | 32.640892 | 16.9 | 4.4 | -191.6 | 4.5 | -1.253 | 0.09 | -1.193 | 0.081 | -0.78 | 0.16 | 0.07 | 0.06 |
| 1315042 | 2867487021995351040 | LAMOST KG | 357.426356 | 30.115 | 16.3 | 2.1 | -197.8 | 3.6 | -0.506 | 0.037 | -1.074 | 0.027 | -0.70 | 0.13 | -0.09 | 0.05 |
| 1315180 | 2867075525473014528 | LAMOST KG | 357.18861 | 41.642576 | 19.0 | 2.1 | -143.9 | 7.3 | -0.949 | 0.088 | -0.944 | 0.057 | -0.39 | 0.25 | 0.08 | 0.08 |
| 1609069 | 375247964054278912 | LAMOST KG | 12.316544 | 29.804014 | 14.4 | 4.0 | -155.4 | 4.3 | -0.602 | 0.077 | -0.403 | 0.069 | -0.47 | 0.27 | 0.09 | 0.08 |
| 7704197 | 311445949992518912 | LAMOST KG | 15.543772 | 30.905615 | 12.2 | 3.1 | -117.3 | 5.2 | -0.794 | 0.057 | -0.716 | 0.052 | -0.60 | 0.17 | 0.11 | 0.06 |

Notes.

S

(This table is available in its entirety in machine-readable form.)

 ^a Unique identifier in LAMOST.
 ^b Solution identifier in Gaia.

| LAMOST | е | Δe | a (kpc) | Δa (kpc) | l _{orb} (deg) | $\Delta l_{ m orb}$ (deg) | b _{orb} (deg) | $\Delta b_{ m orb}$ (deg) | l _{apo} (deg) | $\Delta l_{ m apo}$ (deg) | $\frac{E}{(\text{km}^2 \text{ s}^{-2})}$ | ΔE (km ² s ⁻²) | $\frac{L}{(\text{km s}^{-1} \text{ kpc})}$ | $\frac{\Delta L}{(\text{km s}^{-1} \text{ kpc})}$ |
|---------|-------|------------|------------|------------------|------------------------|---------------------------|------------------------|---------------------------|------------------------|---------------------------|--|---|--|---|
| 216068 | 19.20 | 1.21 | 0.13 | 0.04 | 336.18 | 4.05 | 145.34 | 1.68 | 318.24 | 12.85 | -78274.00 | 1975.62 | 3696.46 | 198.19 |
| 715099 | 19.10 | 3.63 | 0.23 | 0.06 | 326.94 | 13.01 | 155.08 | 0.77 | 322.60 | 73.65 | -78460.68 | 5729.74 | 3555.62 | 661.74 |
| 716170 | 16.91 | 3.66 | 0.13 | 0.06 | 338.98 | 32.60 | 155.52 | 0.66 | 348.73 | 145.56 | -82678.12 | 6309.37 | 3294.14 | 614.95 |
| 1107119 | 21.23 | 3.42 | 0.11 | 0.06 | 351.15 | 148.91 | 162.12 | 1.77 | 355.07 | 143.03 | -76778.87 | 4923.66 | 3892.91 | 544.48 |
| 1202158 | 20.94 | 4.51 | 0.24 | 0.04 | 331.49 | 9.03 | 152.31 | 1.92 | 345.07 | 85.01 | -75428.06 | 6415.99 | 3846.37 | 748.22 |
| 1216219 | 16.16 | 3.19 | 0.28 | 0.06 | 336.28 | 23.05 | 156.04 | 1.71 | 336.99 | 137.39 | -83908.12 | 6040.82 | 3019.25 | 588.88 |
| 1315042 | 15.19 | 1.16 | 0.45 | 0.03 | 335.95 | 8.67 | 153.21 | 0.59 | 269.74 | 64.04 | -85439.85 | 2511.87 | 2571.41 | 218.39 |
| 1315180 | 23.58 | 9.37 | 0.13 | 0.07 | 324.86 | 20.8 | 152.86 | 0.79 | 354.57 | 68.22 | -72894.93 | 9918.26 | 4300.86 | 1264.50 |
| 1609069 | 17.83 | 2.54 | 0.20 | 0.04 | 355.38 | 157.38 | 162.05 | 0.81 | 320.28 | 161.97 | -80862.51 | 4497.49 | 3383.99 | 453.92 |
| 7704197 | 17.23 | 2.73 | 0.13 | 0.03 | 347.19 | 81.99 | 156.75 | 1.01 | 359.75 | 56.65 | -81949.20 | 4950.32 | 3360.89 | 458.79 |

(This table is available in its entirety in machine-readable form.)

6

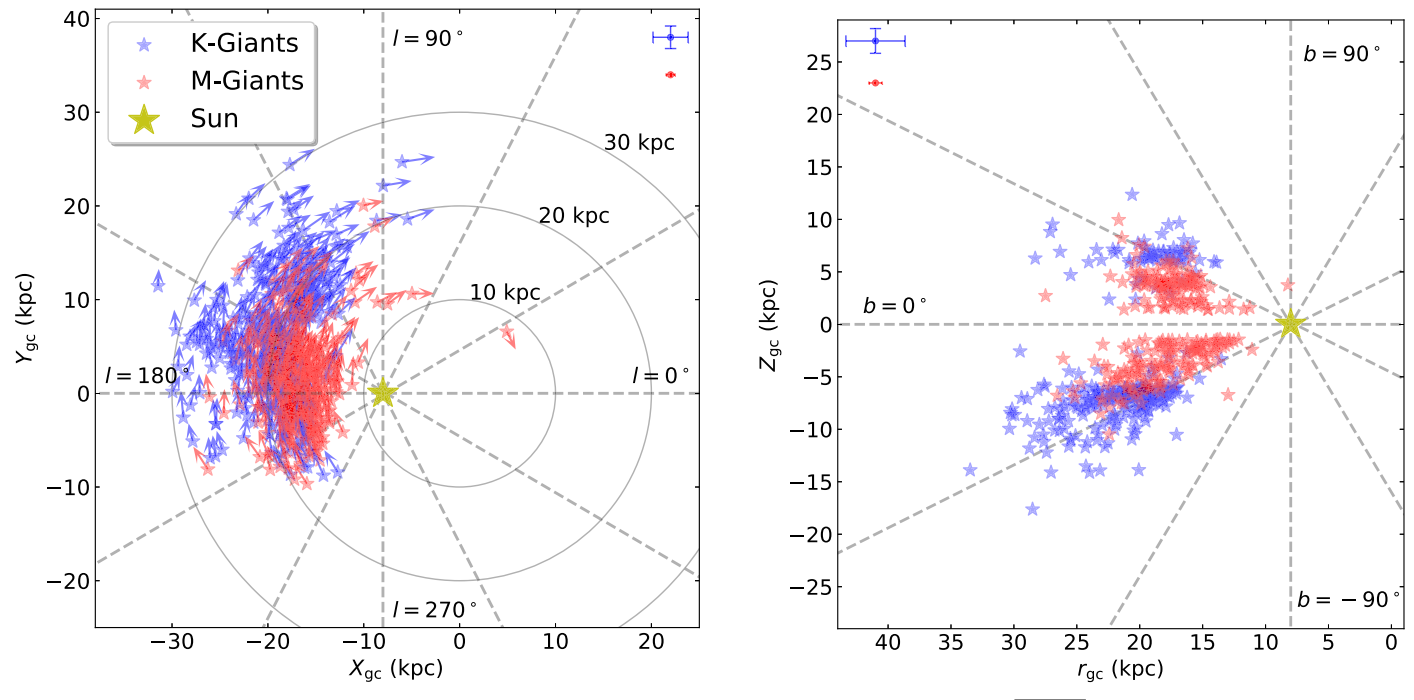


Figure 2. Spatial distribution of the candidates in the X-Y plane (left panel) and R-Z plane (right panel), where $r_{\rm gc} = \sqrt{x^2 + y^2}$. The Galactic center is at (0, 0, 0) and the Sun is at (-8.3, 0, 0) kpc. The Galactic longitude and latitude (dashed) and curves at constant Galactocentric radius (solid) are shown.

velocities in the X-Y plane. We can clearly see that GASS has circular orbits in the X-Y plane. In the right panel, we can see that this structure covers a large range in $r_{\rm gc}$, from 15 out to 30 kpc. This range actually overlaps with the distances and parts of sky areas to Mon, TriAnd, and A13, because there are no clear boundaries between these features. The blue and red error bars in the figure show the mean errors for X, Y, and $Y_{\rm gc}$. Because M giants do not have distance errors for each star, we assign a distance error for M giants with a random function with the relative error restriction equal to 0.05.

Figure 3 shows the spatial distribution of our GASS in the Y-Z plane. In the upper-left panel, the arrows represent the moving direction of all GASS members. We can see a little arc shape in the motion especially in the southern hemisphere. In the remaining three panels, we color-code regions by the mean-V_Z component of the stars' velocities for the samples above/below the plane. From the upper-right panel, we see that the combined K-/M-giant GASS members show a clear V_Z gradient along the Y-axis. The systematical distance error in this work can be ignored because we calibrated the K giants and M giants with Gaia parallax. We also make similar plots for K giants and M giants separately in the lower two panels. From these two subsamples, we can also see a clear V_Z gradient in the Y direction, especially in the M-giant sample, confirming our finding from the combined samples. This behavior could be part of the expected ripple pattern extending out to $r_{\rm gc} > 15 \, \rm kpc$ in Xu et al. (2015) and Li et al. (2017).

Figure 4 shows the line-of-sight velocity distribution for K- and M-giant members of GASS in the northern and southern hemispheres separately. The upper panel shows the northern K- and M-giant groups' line-of-sight velocity distribution, the mean velocities for the K- and M-giant groups are -20.33 and -26.87 km s⁻¹, and the velocity dispersions are 44.08 and 32.32 km s⁻¹. The lower panel shows the southern K- and M-giant groups' line-of-sight velocity distribution, the mean

velocities for K and M giants are 17.91 and 16.27 km s⁻¹, and the velocity dispersions are 17.31 and 28.86 km s⁻¹. The typical line-of-sight velocity dispersion for the thick disk is around 30–40 km s⁻¹ (Bensby et al. 2003; Li et al. 2012; Bensby et al. 2014). The velocity dispersion for the thin disk is smaller than 20 km s⁻¹ (Bensby et al. 2003, 2014). It is hard to simply compare our results to thin and thick disks; there are obviously different velocity dispersions for the northern and southern parts of our GASS, but on the whole, the velocity dispersion of the northern groups is much larger than that of the southern groups. This asymmetric structure could be related to the disk ripple/wave structure as expected or detected by previous work (Carlin et al. 2013; Xu et al. 2015, 2020; Li et al. 2017; Wang et al. 2018, 2020).

3.3. Comparison of Dynamical Properties with the Disk Population

Figure 5 shows the E versus L_z distribution for the GASS members (red stars), disk stars (yellow and purple density background) chosen from our K-giant sample for which |Z| < 3 kpc, and Sagittarius stream members selected from Yang et al. (2019b; green circles). From the density background, we can clearly see two components: the yellow region is attributed to thin-disk stars, and the purple region is attributed to thick-disk stars. ¹⁴ As we can see, the E versus L_z distribution of our GASS members is totally different from that of the thick disk and Sagittarius stream. It is located in an extended narrow region of thin-disk stars but has a higher E and lower L_z value than most of the thin-disk population.

 $[\]overline{\ }^{14}$ The thin- and thick-disk stars naturally separate in the [M/H] versus [α /M] diagram as shown in Figure 7. We selected the relatively pure thin- and thick-disk stars within the 1σ distribution for the density distribution of the distinct thick- and thin-disk clumps in Figure 7, and checked where these pure thin- and thick-disk star distributions are in the E versus L_{τ} figure.

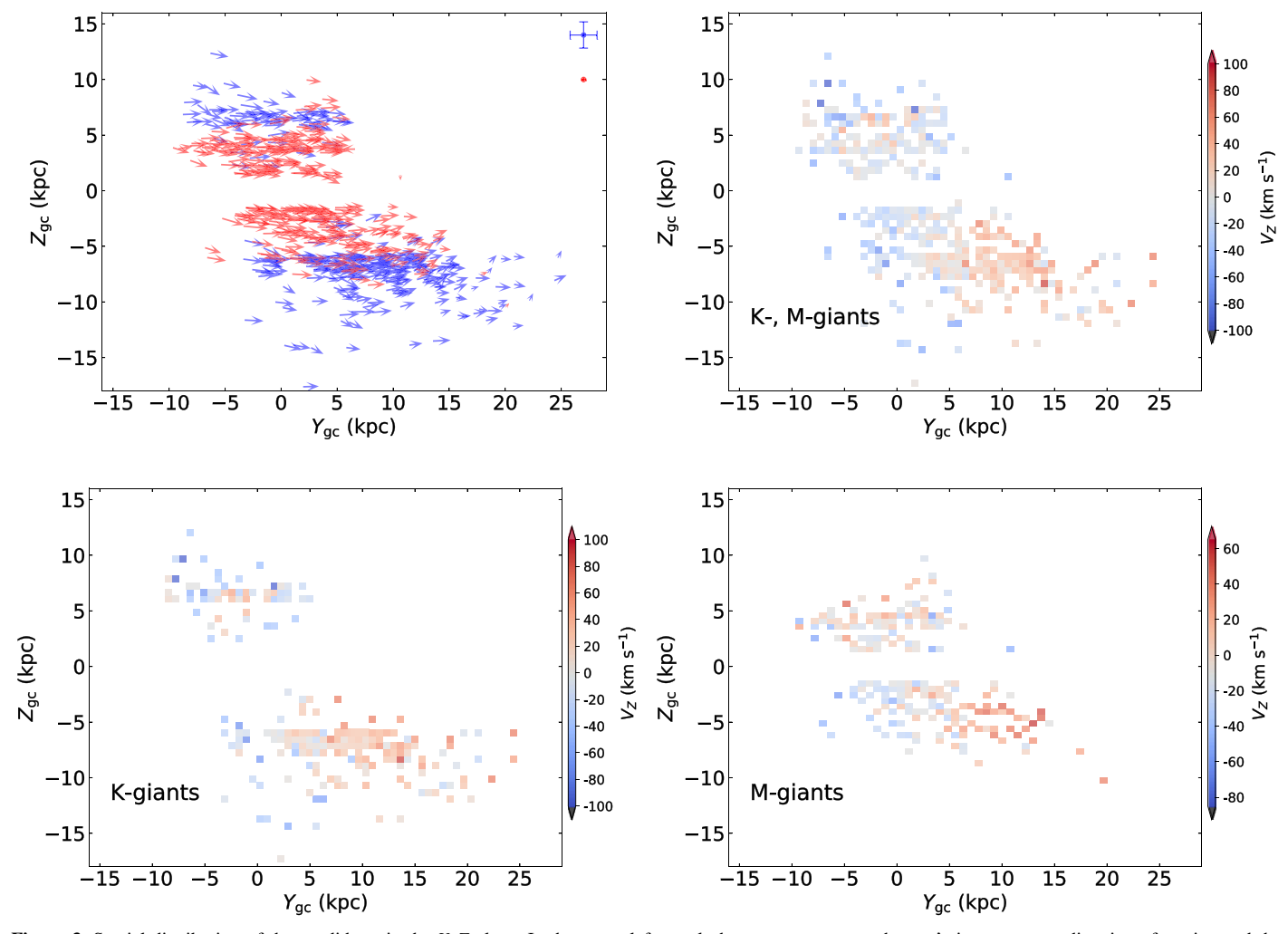


Figure 3. Spatial distribution of the candidates in the Y-Z plane. In the upper-left panel, the arrows represent the star's instantaneous direction of motion and the velocity amplitudes. In the other panels, the color shows the mean V_Z in each bin in Y-Z space. We can clearly see the V_Z gradient along the Y-axis. Considering that there could be systematic distance errors between the K and M giants that might affect the oscillation, we illustrate the K- and M-giant mean- V_Z density maps separately in the lower panels, where the effect is still present.

4. The Chemical Abundance Features of GASS

4.1. The Metallicity Distribution

The [M/H] for all K-/M-giant members spans a large distribution from -1.50 to 0.25, with the mean metallicity around -0.56 dex, and metallicity dispersion around 0.22 dex as shown in Figure 6. From the upper panel, we see that all of the K and M giants have similar [M/H] distributions. The lower panel shows the distributions of the northern and southern structures separately, which also have similar [M/H] distributions. For both K and M giants, 90% of members have [M/H] values larger than -1. Earlier works about Mon or other anticenter structures suggested they could be the remnants of dwarf galaxies that merged with the outer disk, but for most Milky Way satellites or dwarf galaxies, the mean stellar metallicities are much smaller than -1.5 dex (McConnachie 2012; Simon 2019). Considering that the metallicity and E versus L_z distribution of our GASS are far from the dwarf galaxies' distribution, we infer it is unlikely the remnants of dwarf galaxies that merged in the Milky Way's outer disk.

This [M/H] distribution is similar to that found by Chou et al. (2010) from high-resolution spectra of 21 M-giant stars.

This confirms that the groups in the north and south likely belong to one larger group.

4.2. The α -abundance Distribution

Figure 7 presents the α -element abundances $[\alpha/M]$ for the LAMOST K and M giants obtained by SLAM (Zhang et al. 2019). To compare with the Galactic disk and halo stars, we choose disk stars from LAMOST K giants with |Z| < 3 kpc (blue density map in Figure 7, which naturally separates into thin- and thick-disk stars in $[\alpha/M]$ versus [M/H] space), and for halo stars, we select |Z| > 5 kpc and eliminate the substructures (blue dots; X.-X. Xue et al. 2021, in preparation). As we can see, our GASS members have similar α -element abundances $[\alpha/M]$ to the thin disk, but are more metal-poor than typical thin-disk stars. This result is consistent with the continuation of metal-rich thin-disk stars into the outer halo (Haywood et al. 2016). It is also consistent with the α abundance derived in Hayes et al. (2018) for the TriAnd substructure, which suggests that this feature is an "extension" of the trend seen in the disk.

We infer that our GASS members may be part of the outer disk, representing a transition population between the thin disk,

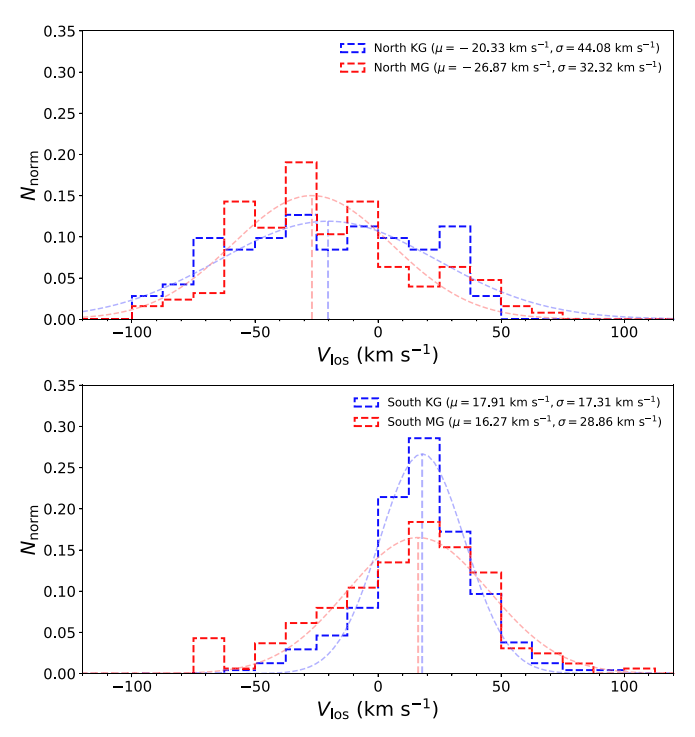


Figure 4. Line-of-sight velocity distribution for K- and M-giant members of GASS in the north and south hemispheres separately. The red and blue dashed lines show the Gaussian distribution for each group, with the mean velocities and velocity dispersion shown in the figure.

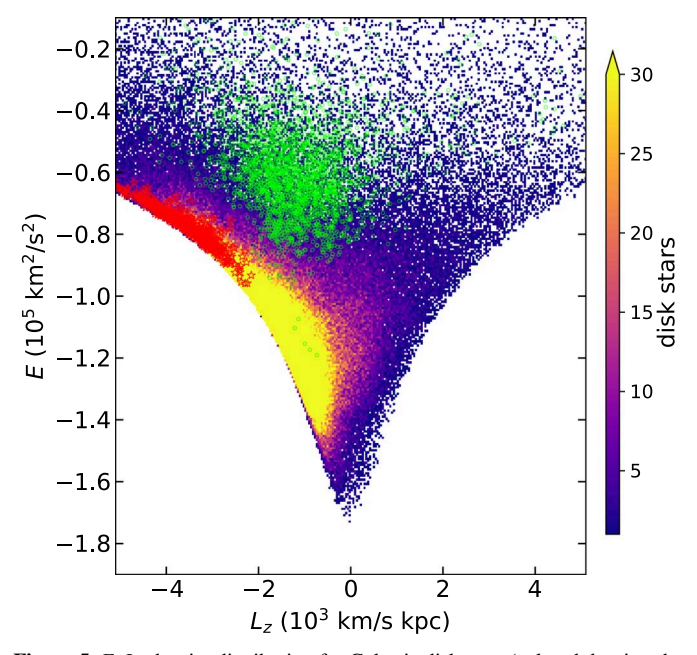


Figure 5. $E-L_Z$ density distribution for Galactic disk stars (colored density; the data are from the K-giant catalog with |Z| < 3 kpc.), GASS members (red stars), and Sagittarius stream members selected from Yang et al. (2019b; green circles).

thick disk, and halo. Figure 8 shows K-giant stars selected in the same Galactic distance range as GASS, separated into two samples with $15 < r_{\rm GC} < 25$ kpc and a more nearby "outer disk" sample between $10 < r_{\rm GC} < 15$ kpc. These data are taken from the LAMOST K-giant catalog, but removed all of the groups identified in X.-X. Xue et al. (2021, in preparation) to get a pure sample from the disk and halo. We split these stars

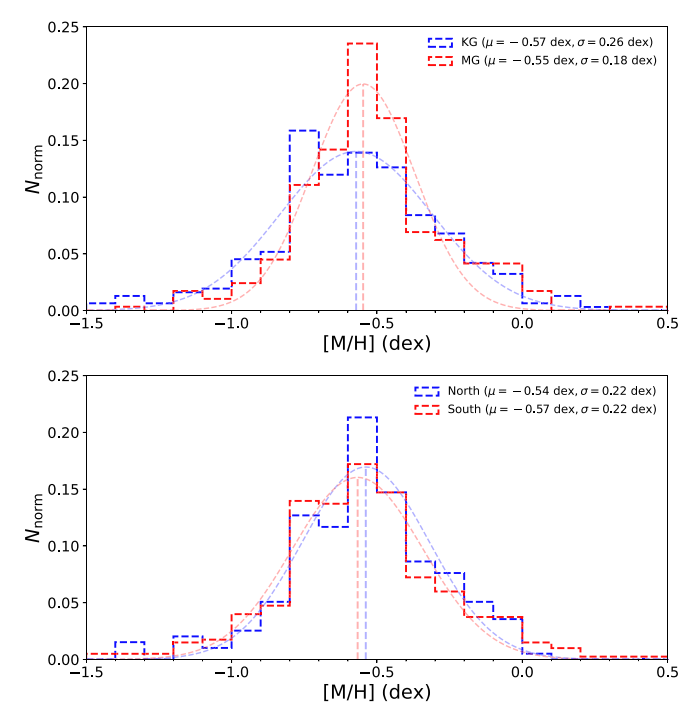


Figure 6. Metallicity distribution for our GASS members. The left panel shows a comparison between the M giants (red line) and the K giants (blue dash line). The right panel shows the comparison between the southern and northern samples.

into three groups: 7 < |Z| < 12 kpc, 2 < |Z| < 7 kpc, and a disk sample at -2 < Z < 2 kpc. In the upper panel, in the distance range from 10 to 15 kpc, we can see a clear clump of thin-disk stars with |Z| < 2 kpc. From 2 < |Z| < 7 kpc, there are still some thin-disk stars, but we can also see the clump of the thickdisk star sequence. Cheng et al. (2012) has suggested that the scale length of the thick disk is quite short, not much more than 2 kpc, whereas traditionally a 3 kpc scale length was assumed. Our result seems to agree that, in the range $10 < r_{GC} < 15$ kpc, |Z| < 2 kpc is not related to the thick disk at all. In the lower panel, showing a distance range from 15 to 25 kpc, we can see that the thin-disk stars (|Z| < 2 kpc) are clearly reduced compared to the more nearby sample. For stars 2 < $|Z| < 7 \,\mathrm{kpc}$, the thick-disk star sequence has disappeared (yellow dots; $\lceil \alpha/M \rceil > 0.2$ clump in the upper panel), but the lower sequence still exists, which is similar to the locus of our GASS members in the [M/H]– $[\alpha/M]$ space.

We infer that this sequence could be the transition sequence between the thin-disk-thick-disk halo. Comparing these two distance ranges, we can see a clear variation in [M/H]–[α /M] space within 2 < |Z| < 7 kpc. We also see that most thick-disk stars appear in the 10 kpc < $R_{\rm GC}$ < 15 kpc range with 2 < |Z| < 7 kpc.

In previous work, Liu et al. (2017) and Wang et al. (2018) have shown through stellar density profiles that the Galactic disk is more extended than previously thought, reaching out to $R \sim 19$ kpc. In Figure 3, Haywood et al. (2016) show that there is an inner disk composed of thick-disk and metal-rich thin-disk stars. The α abundance of 12 TriAnd substructure member stars derived in Hayes et al. (2018) shows a similar distribution to our GASS in $[\alpha/M]$ versus [M/H] space; we note that Hayes et al. also claimed TriAnd is an "extension" of the disk.

We also compare our GASS with MWTD; the eccentricities *e* of MWTD are smaller than 0.4, and all our GASS have

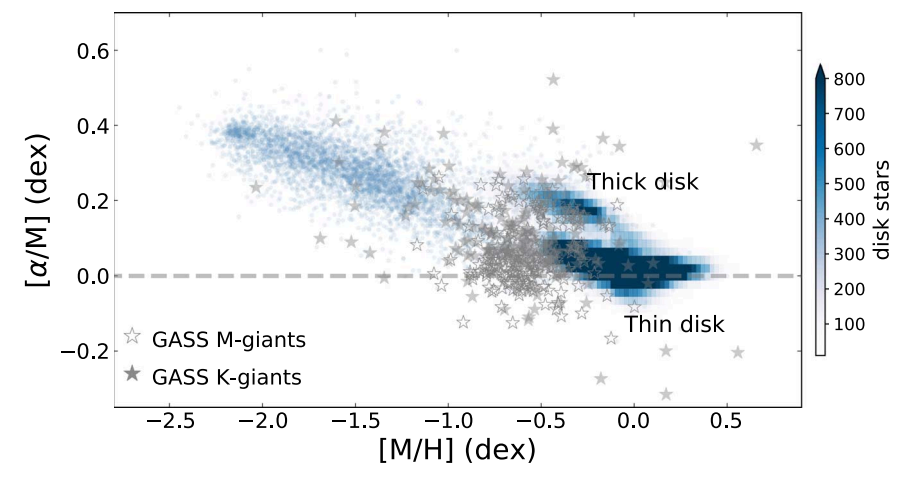


Figure 7. [\(\alpha\)/H] distribution of stars from GASS (gray stars), compared to the thick-disk, thin-disk, and halo stars (blue density).

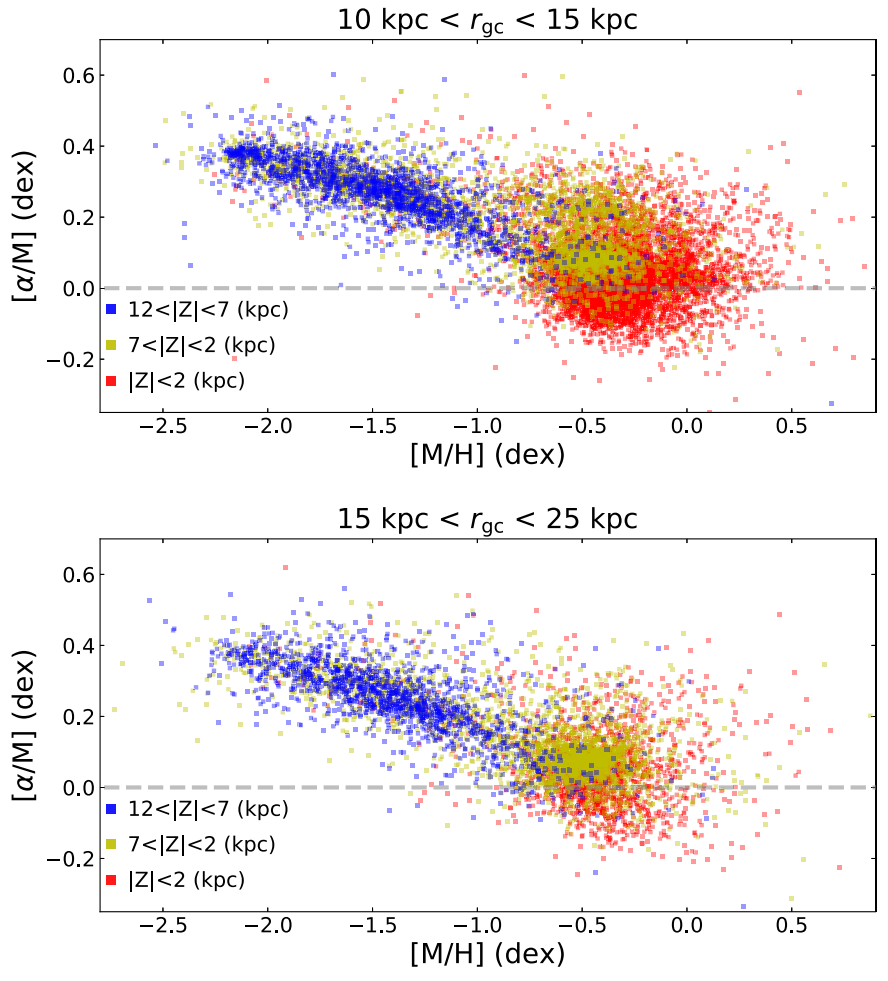


Figure 8. $[\alpha/\mathrm{M}]$ vs. $[\mathrm{M/H}]$ distribution of the K-giant sample. The upper panel shows all stars selected between $10 < r_{\mathrm{GC}} < 15$ kpc but we have subtracted the group members identified in X.X. Xue et al. (2021, in preparation), and then split into samples of different distances to the Galactic plane: 7 < Z < 12 kpc, 2 < Z < 7 kpc, -7 < Z < -2 kpc, and -12 < Z < -7 kpc, and a "disk" sample at -2 < Z < 2 kpc. The lower panel is similar to the upper panel but for a different distance range of $15 < r_{\mathrm{GC}} < 25$ kpc.

e < 0.35. The metallicity of MWTD is similar to our GASS; previously detected MWTD are all in the solar neighborhood, but our GASS are much farther away. Anyway, except for the distance range, the chemical abundance, kinematic feature, and eccentricity of our GASS are all very similar to those of MWTD.

Based on the evidence we have presented, we infer that the outer-disk sequence represents a different evolution, where the outer Milky Way still has more cold gas in the present day and then maybe lower star-formation efficiency than the inner disk. Our GASS members are could be part of the outer metal-poor disk stars, and the outer disk could extend to 30 kpc.

5. Discussion and Conclusions

By combining the IoM and FoF algorithms, X.-X. Xue et al. (2021, in preparation) selected 589 GASS K- and M-giant stars from LAMOST DR5 in the Galactic anticenter region based on their similar kinematic and chemical abundance features. These stars cover a large range in r_{gc} , but have similar angular momentum and energy distributions, which could be related to the previously identified substructures Mon, TriAnd, and A13, which we have collectively named the Galactic anticenter substructure (GASS).

Based on this sample, we present observations including kinematic and chemical parameters of these stars in Table 1 and the calculated orbit parameters in Table 2. All the members are published in machine-readable catalogs.

The GASS covers a large area of the sky, centered around the Galactic anticenter region on both sides of the Milky Way disk, in a Galactic longitude range from 80° to 230°, while the Galactic latitude goes from -35° to 40° . This coverage is in good positional alignment with the "band-like" structures detected in the Pan-STARRS map, especially the highlighted features B, C, and D in Figure 3 of Slater et al. (2014).

The velocity vector directions of GASS in the X-Y and Y-Zplanes indicate that the GASS consists of two circular orbits on both sides of the Milky Way disk which span a large distance from 15 to 30 kpc. We can see a clear velocity gradient on the Y-Z plane as shown in Figure 3, with V_Z pointing toward and outward from the midplane at different distances in the southern hemisphere. We also compared our GASS stars to the disk and Sagittarius stream in $E-L_{\tau}$ space. GASS members have a similar *L–E* distribution to the thin-disk distribution.

We also present the metallicity distribution of GASS. The total [M/H] distributions for K- and M-giant GASS members are similar. We did not find significant [M/H] differences for the GASS southern and northern rings. By comparing the α abundance with the Galactic components, the trend of $[\alpha/M]$ is not the same as the traditional Galactic disk or halo populations. The GASS distribution in $[\alpha/M]$ versus [M/H]space is consistent with the continuation of metal-rich thin-disk stars into the outer halo (Haywood et al. 2016). It is also consistent with the α abundance derived in Hayes et al. (2018) for the TriAnd substructure, which suggests that this feature is an "extension" of the trend seen in the disk.

Our analysis shows that Mon, TriAnd, and A13 (and possibly including other stars near the Galactic anticenter) have similar kinematic and chemical features. These stars may be just part of the outer disk, with this outer disk extending out to at least $r_{\rm gc}$ \sim 30 kpc. GASS may have formed in the outer disk where there may still be more cold gas in the present day and then maybe lower star-formation efficiency than the inner disk. We can also infer that the GASS stars may have formed after the thick disk was formed because the molecular cloud density decreased in the outer disk, where the star-formation rate might be less efficient compared to the inner disk.

This work is supported by the National Key R&D Program of China under grant No. 2019YFA0405500; by NSFC grant Nos. 11988101, 11873052, 11890694, 11835057, 11703019, 11503066, U1731129, 11703038, and 11773033; and by China West Normal University grants 17C053, 17YC507, and 16EE018. J.L.C. acknowledges support from HST grant HST-GO-15228.001-A and NSF grant AST-1816196. R.A.M. acknowledges support from the Chilean Centro de Excelencia en Astrofisica y Tecnologias Afines (CATA) BASAL AFB-170002, and FONDECYT/CONICYT grant # 1190038. This work is sponsored (in part) by the Chinese Academy of Sciences (CAS), through a grant to the CAS South America Center for Astronomy (CASSACA) in Santiago, Chile.

Guoshoujing Telescope (the Large Sky Area Multi-Object Fiber Spectroscopic Telescope LAMOST) is a National Major Scientific Project built by the Chinese Academy of Sciences. Funding for the project has been provided by the National Development and Reform Commission. LAMOST is operated and managed by the National Astronomical Observatories, Chinese Academy of Sciences.

This work is sponsored by the Cultivation Project for LAMOST Scientific Payoff and Research Achievement of CAMS-CAS.

This work has made use of data from the European Space Agency (ESA) mission Gaia (https://www.cosmos.esa.int/ gaia), processed by the Gaia Data Processing and Analysis Consortium (DPAC, https://www.cosmos.esa.int/web/gaia/ dpac/consortium). Funding for the DPAC has been provided by national institutions, in particular the institutions participating in the Gaia Multilateral Agreement.

ORCID iDs

```
Jing Li https://orcid.org/0000-0002-4953-1545
Xiang-Xiang Xue https://orcid.org/0000-0002-0642-5689
Chao Liu https://orcid.org/0000-0002-1802-6917
Bo Zhang https://orcid.org/0000-0002-6434-7201
Hans-Walter Rix https://orcid.org/0000-0003-4996-9069
Jeffrey L. Carlin https://orcid.org/0000-0002-3936-9628
Chengqun Yang https://orcid.org/0000-0003-1972-0086
Jing Zhong https://orcid.org/0000-0001-5245-0335
Hao Tian https://orcid.org/0000-0003-3347-7596
Yan Xu https://orcid.org/0000-0002-2459-3483
Gang Zhao https://orcid.org/0000-0002-8980-945X
```

```
References
An, D., Beers, T. C., Johnson, J. A., et al. 2013, ApJ, 763, 65
Antoja, T., Helmi, A., Romero-Gómez, M., et al. 2018, Natur, 561, 360
Arifyanto, M. I., Fuchs, B., Jahreiß, H., et al. 2005, A&A, 433, 911
Bailer-Jones, C. A. L., Rybizki, J., Fouesneau, M., Mantelet, G., & Andrae, R.
  2018, AJ, 156, 58
Beers, T. C., Carollo, D., Ivezić, Ž., et al. 2012, ApJ, 746, 34
Beers, T. C., Chiba, M., Yoshii, Y., et al. 2000, AJ, 119, 2866
Beers, T. C., Norris, & Sommer-Larsen, J. 1995, ApJS, 96, 175
Beers, T. C., Norris, J. E., Placco, V. M., et al. 2014, ApJ, 794, 58
Beers, T. C., & Sommer-Larsen, J. 1995, ApJS, 96, 175
Bensby, T., Feltzing, S., & Lundström, I. 2003, A&A, 410, 527
Bensby, T., Feltzing, S., & Oey, M. S. 2014, A&A, 562, A71
Bidelman, W. P., & MacConnell, D. J. 1973, AJ, 78, 687
Binney, J., & Schönrich, R. 2018, MNRAS, 481, 1501
Bird, S. A., Xue, X.-X., Liu, C., et al. 2019, AJ, 157, 104
Bland-Hawthorn, J., Sharma, S., Tepper-Garcia, T., et al. 2019, MNRAS,
Carlin, J. L., DeLaunay, J., Newberg, H. J., et al. 2013, ApJL, 777, 5
Carollo, D., Beers, T. C., Bovy, J., et al. 2012, ApJ, 744, 195
Carollo, D., Beers, T. C., Chiba, M., et al. 2010, ApJ, 712, 692
Carollo, D., Beers, T. C., Lee, Y. S., et al. 2007, Natur, 450, 1020
Carollo, D., Freeman, K., Beers, T. C., et al. 2014, ApJ, 788, 180
Carraro, G., & Costa, E. 2009, A&A, 493, 71
Cheng, J. Y., Rockosi, C. M., Morrison, H. L., et al. 2012, ApJ, 752, 51
Cheng, X., Liu, C., Mao, S., et al. 2019, ApJL, 872, L1
Chiba, M., & Yoshii, Y. 1998, AJ, 115, 168
Chou, M.-Y., Majewski, S. R., Cunha, K., et al. 2010, ApJL, 720, L5
Cui, X.-Q., Zhao, Y.-H., Chu, Y.-Q., et al. 2012, RAA, 12, 1197
de Grijs, R., & Bono, G. 2016, ApJS, 227, 5
de Grijs, R., & Bono, G. 2017, ApJS, 232, 22
```

```
Deason, A. J., Belokurov, V., Hamren, K. M., et al. 2014, MNRAS, 444, 3975
Deng, L.-C., Newberg, H. J., Liu, C., et al. 2012, RAA, 12, 735
Feast, M. W., Menzies, J. W., Matsunaga, N., & Whitelock, P. A. 2014, Natur,
  509, 342
Gaia Collaboration, Brown, A. G. A., Vallenari, A., et al. 2018, A&A, 616, A1
Gilmore, G., Wyse, R. F. G., & Norris, J. E. 2002, ApJL, 574, L39
Gómez, F. A., White, S. D. M., Marinacci, F., et al. 2016, MNRAS, 456, 2779
Hammersley, P. L., & López-Corredoira, M. 2011, A&A, 527, A6
Hayes, C. R., Majewski, S. R., Hasselquist, S., et al. 2018, ApJL, 859, L8
Haywood, M., Lehnert, M. D., Di Matteo, P., et al. 2016, A&A, 589, A66
Villalobos, Á., & Helmi, A. 2009, MNRAS, 399, 166
Ibata, R. A., Irwin, M. J., Lewis, G. F., Ferguson, A. M. N., & Tanvir, N. 2003,
       RAS, 340, L21
Ji, W., Cui, W., Liu, C., et al. 2016, ApJS, 226, 1
Laporte, C. F. P., Gómez, F. A., Besla, G., et al. 2018, MNRAS, 473, 1218
Laporte, C. F. P., Minchev, I., Johnston, K. V., & Gómez, F. A. 2019,
       RAS, 485, 3134
Li, J., Newberg, H. J., Carlin, J. L., et al. 2012, ApJ, 757, 151
Li, J., Smith, M. C., Zhong, J., et al. 2016, ApJ, 823, 59
Li, T. S., Sheffield, A. A., Johnston, K. V., et al. 2017, ApJ, 844, 74
Li, Y.-B., Luo, A.-L., Du, C.-D., et al. 2018, ApJS, 234, 31
Liu, C., Deng, L.-C., Carlin, J. L., et al. 2014, ApJ, 790, 110
Liu, C., Wang, Y.-G., Shen, J., et al. 2017, ApJL, 835, L18
López-Corredoira, M., Cabrera-Lavers, A., Garzón, F., & Hammersley, P. L.
  2002. A&A. 394. 883
Luo, A.-L., Zhang, H.-T., Zhao, Y.-H., et al. 2012, RAA, 12, 1243
Majewski, S. R., Schiavon, R. P., Frinchaboy, P. M., et al. 2017, AJ, 154, 94
Martin, J. C., & Morrison, H. L. 1998, AJ, 116, 1724
McConnachie, A. W. 2012, AJ, 144, 4
Meisner, A. M., Frebel, A., Jurić, M., & Finkbeiner, D. P. 2012, ApJ, 753, 116
Moitinho, A., Vázquez, R. A., Carraro, G., et al. 2006, MNRAS, 368, L77
Momany, Y., Zaggia, S., Gilmore, G., et al. 2006, A&A, 451, 515
```

```
Morrison, H. L., Flynn, C., & Freeman, K. C. 1990, AJ, 100, 1191
Morrison, H. L., Helmi, A., Sun, J., et al. 2009, ApJ, 694, 130
Newberg, H. J., & Carlin, J. L. 2016, Tidal Streams in the Local Group and
   Beyond: Observations and Implications, Vol. 420, Astrophysics and Space
  Science Library (Cham: Springer)
Newberg, H. J., Yanny, B., Rockosi, C., et al. 2002, ApJ, 569, 245
Norris, J., Bessell, M. S., & Pickles, A. J. 1985, ApJS, 58, 463
Rocha-Pinto, H. J., Majewski, S. R., Skrutskie, M. F., & Crane, J. D. 2003,
   ApJL, 594, L115
Schönrich, R., Binney, J., & Dehnen, W. 2010, MNRAS, 403, 1829
Sharma, S., Johnston, K. V., Majewski, S. R., et al. 2010, ApJ, 722, 750
Sheffield, A. A., Price-Whelan, A. M., Tzanidakis, A., et al. 2018, ApJ, 854, 47
Simon, J. D. 2019, ARA&A, 57, 375
Slater, C. T., Bell, E. F., Schlafly, E. F., et al. 2014, ApJ, 791, 9
Steinmetz, M., Zwitter, T., Siebert, A., et al. 2006, AJ, 132, 1645
Tian, H.-J., Liu, C., Wu, Y., et al. 2018, ApJL, 865, L19
Wang, H.-F., Liu, C., Xu, Y., et al. 2018, MNRAS, 478, 3367
Wang, H.-F., López-Corredoira, M., Huang, Y., et al. 2020, MNRAS,
  491, 2104
Xu, Y., Liu, C., Tian, H., et al. 2020, ApJ, 905, 6
Xu, Y., Newberg, H. J., Carlin, J. L., et al. 2015, ApJ, 801, 105
Xue, X.-X., Ma, Z., Rix, H.-W., et al. 2014, ApJ, 784, 170
Yang, C., Xue, X.-X., Li, J., et al. 2019a, ApJ, 886, 154
Yang, C., Xue, X.-X., Li, J., et al. 2019b, ApJ, 880, 65
Yanny, B., & Newberg, H. J. 2016, in Tidal Streams in the Local Group and
   Beyond: Observations and Implications, Vol. 420, Astrophysics and Space
   Science Library, ed. H. J. Newberg & J. L. Carlin (Cham: Springer), 63
Yanny, B., Newberg, H. J., Grebel, E. K., et al. 2003, ApJ, 588, 824
York, D. G., Adelman, J., Anderson, J. E., et al. 2000, AJ, 120, 1579
Zhang, B., Liu, C., & Deng, L. C. 2019, arXiv:1908.08677
Zhao, G., Zhao, Y.-H., Chu, Y.-Q., et al. 2012, RAA, 12, 723
Zhong, J., Li, J., Carlin, L. J., et al. 2019, ApJS, 244, 8
```